World Electric Vehicle Journal

MDPI

Article

Analysis of Heating System Impacts on Battery Electric Vehicle Operation at Cold Temperatures †

Kieran Humphries * and Aaron Loiselle-Lapointe

Transportation Emissions and Electrification Laboratory, Environment and Climate Change Canada, Ottawa, ON K1V 1C7, Canada; aaron.loiselle@ec.gc.ca

* Correspondence: kieran.humphries@ec.gc.ca

† This paper is a revised and expanded version of the conference paper "A Comparison of Heat Pump and Resistive Heating Impacts on Battery Electric Vehicle Energy Consumption and Range in Cold Temperatures", presented at EVS38 in Gothenburg, Sweden in June 2025.

Abstract

This paper presents the results from in-lab chassis dynamometer testing of two battery electric vehicles of the same make and model: a 2022 model year vehicle with a heat pump and a 2020 model year vehicle with a resistive positive temperature coefficient (PTC)-type heater. The vehicles were tested over a series of standard drive cycles at −10 °C, −7 °C, 0 °C, and 25 °C to determine the impacts of the different heating systems on vehicle energy consumption and driving range in cold temperatures. The results indicate that in most (but not all) heating situations the heat pump heated its vehicle's cabin more efficiently than the PTC heater did, especially at 0 °C. At the lowest temperature, −10 °C, the heat pump used more energy than the PTC heater on cold-start but was more efficient than the PTC heater once the cabin was warmed up. Over standard drive cycles and using SAE J1634 calculation methods to obtain a single range value for each cycle type, the improvement in the percentage of driving range retained by the heat pump-equipped vehicle over the PTC heater-equipped vehicle varied between 1% and 15% depending on ambient conditions and drive cycle, with the average advantage in percentage range retained being 7% over the UDDS cycle, 7% over the HWFET cycle, and 4% over the US06 cycle for all cold temperatures combined.

Keywords: electric vehicles; thermal management; energy management; heat pump; PTC heater; resistive heating

Check for updates

Academic Editors: Joeri Van Mierlo and Peter Van den Bossche

Received: 5 February 2026
Revised: 8 March 2026
Accepted: 10 March 2026
Published: 25 March 2026

Copyright: © 2026 His Majesty, the King in Right of Canada, as represented by the Minister of the Environment. Published by MDPI on behalf of the World Electric Vehicle Association. Licensee MDPI, Basel, Switzerland. This article is an open access article distributed under the terms and conditions of the Creative Commons Attribution (CC BY) license.

1. Introduction

This paper is a revised and expanded version of the conference paper presented at EVS38 in Gothenburg, Sweden in June 2025 [1], in which two different heating systems for electric vehicles were compared.

Battery electric vehicles (BEVs) operating in cold conditions are at an inherent disadvantage when compared to conventional internal combustion engine (ICE) vehicles, as they do not have a readily available source of waste heat with which to heat their cabins. ICE vehicles produce a significant amount of waste heat while driving, and this allows them to heat their cabins in cold conditions without using additional stored energy (fuel) to do so. On the other hand, BEV drivetrains are extremely efficient and do not produce enough waste heat to usefully heat the cabin via traditional forced-air systems. Instead, BEVs must use the on-board battery energy storage system (BESS) to produce heat for the cabin, and this reduces the available energy in the BESS to power the propulsion system, thus lowering

the BEV's overall efficiency and driving range [2]. Since their worldwide debut in the 2010s, lithium-ion battery-powered BEVs have employed resistive electrical heating systems to heat their cabins in cold weather [3,4]. Resistive heating options in BEVs include Positive Temperature Coefficient (PTC)-type heaters positioned directly inside cabin ventilation ducts and liquid coolant heaters that provide heated coolant to a heater core within these ducts [5]. In either case, resistive heaters can draw a significant load from the battery under cold ambient conditions, leading to high energy use and less available energy for driving [6–10]. This issue was recognized by BEV drivers and the automotive industry after the release of the first lithium-ion battery-powered BEVs, with many enthusiastic early-adopters discussing their experiences, their workarounds and ad hoc solutions on forums, such as My-iMiEV, My Nissan Leaf Forum, "diyelectriccar" and others [11–13]. Researchers and the industry began proposing alternatives to energy-hungry resistive heaters, alternatives such as infrared heating and heat pumps [14–17]. Heat pumps have recently emerged as the preferred alternative heating technology for BEVs and have been implemented as a standalone solution or in concert with PTC heaters in many BEVs sold worldwide today [2,18]. In Canada's cold climate, cabin heating is a particularly pressing issue for potential buyers of BEVs, so much so that some vehicles sold without advanced heating strategies in other countries are sold with heat pumps and 'winterized' packages as a standard trim option (or in some cases higher trim options) in Canada [19]. Numerous studies have been conducted in recent years that explore the performance of different heat pump designs and configurations in BEVs and are summarized and compared in published literature reviews [5,6,20].

The Tesla Model 3 is an example of a BEV with an HVAC system that has undergone several modifications over its production run, including a significant update to its heating system in 2021. Early versions of the vehicle use a dedicated PTC heater for cabin heating. This heater is located directly in the incoming cabin air stream and heats the air prior to it exiting the ventilation vents. A model update in 2021 saw the inclusion of an advanced heating system that uses a heat pump and additional hardware, resulting in a complex heating system with many operating modes [21,22]. These modes allow the heat pump to scavenge heat from the ambient air (as is typical of an air-source heat pump system) and to collect waste heat from some of the vehicle's components [21,22]. In addition, as detailed in the manufacturer's patent filings, the heat pump system can run in a so-called "lossy mode" when temperatures are very cold, which allows it to produce heat directly by running the heat pump compressor (avoiding the need for a backup PTC heater, unlike in most other electric vehicle models with heat pump systems) [21,22]. This substantial modification to this vehicle model's heating system between model years offers a unique opportunity to compare the cold weather performance of the same model of BEV with and without a heat pump system.

This study quantifies and compares the energy consumption and range retention results of both a PTC heater-equipped vehicle and a heat pump-equipped vehicle in cold temperatures. As noted previously, this is an important topic for Canadian consumers, regulators, and manufacturers selling vehicles in Canada, as range anxiety in cold weather is a barrier to BEV adoption in northern countries. This study uses experimental methods based on certification-type chassis dynamometer testing of vehicles instead of computer modeling to make this comparison between heating system types. The facilities required for this type of study are rare throughout North America and the world, and therefore other experimental studies directly of this type and on the topic of BEV heating systems are not common. This research aims to begin to fill this gap.

2. Materials and Methods

In the fall of 2022, the two test vehicles were tested on an AWD chassis dynamometer with a 1.22 m (48″) roll diameter over the same test conditions and sequences at the Transportation Emissions and Electrification Laboratory (TEEL) in Ottawa, Canada. The procedure followed the Short Multi-Cycle Test Plus Steady-State (SMCT+) sequence, as outlined in the SAE J1634 Recommended Practice [23]. Both vehicles underwent testing at −10 °C, −7 °C, 0 °C, and 25 °C to evaluate the results at different ambient conditions. A temperature of −10 °C was chosen for testing as this was the coldest test condition possible in this facility, while −7 °C and 25 °C were chosen since these are the standard test conditions for chassis dynamometer testing of vehicles. A temperature of 0 °C was added as an intermediate condition where heating use would be expected but its effect on energy consumption would be reduced. Energy consumption and estimated range results were calculated for both vehicles at each temperature condition. A picture of one of the vehicles being tested on the chassis dynamometer is shown in Figure 1.



Figure 1. Test vehicle 1 (model year 2020) being driven on the AWD chassis dynamometer, with variable speed fan in front.

2.1. Vehicle Specifications

Two Tesla Model 3s of the same trim configuration but of two different model years were selected for this study, one using a PTC heater and one using a heat pump for cabin heating, allowing a rare comparison of these different heating systems in operation. Vehicle #1 is the model year 2020 vehicle and includes the initially offered PTC (resistive) heater for cabin heating. Vehicle #2 is the model year 2022 vehicle and uses the advanced heat pump system for cabin heating that is now standard on this model. General specifications of each vehicle are listed in Table 1. Note that battery capacity was changed between these model years, as well as the drive motors' power outputs. These discrepancies were accounted for in the analysis by normalizing the calculated changes in range between ambient temperatures to each individual vehicle's calculated range at 25 °C, as reported in Section 3.8.

Table 1. Test vehicle specifications.

Parameter	Vehicle #1	Vehicle #2
Cabin Heating Type	PTC heater	Heat pump
Refrigerant Type	R134a (for air conditioner)	R1234yf
Make	Tesla	Tesla
Model	Model 3 Long Range AWD	Model 3 Long Range AWD
Model Year	2020	2022
Manufacturing Date	01/20	11/21
Curb Weight (lb)	4033	4052
GVWR (lb)	5072	4883
Equivalent Test Weight (lb)	4250	4250
Motor Power Front/Rear (kW) [24]	147/188	98/195
Battery Description	Lithium-ion, NCA cathode	Lithium-ion, NCA cathode
Rated Battery Capacity (kWh)	75 [25]	82 [26]
UBE from Certification (kWh)	79.8 [27]	82.1 [28]
Rated Electric Range (km) [29]	518	576
Unadjusted Energy Consumption (DC Wh/km) (UDDS/HWFET)	105/112 [27]	101/108 [28]
Tire Make/Model (OEM)	Michelin Primacy	Michelin Primacy
Tire Size	235/45R18	235/45R18
Cold Tire Pressure (psi)	42	42

2.2. Individual Drive Cycles

The standard drive cycles specified in J1634 for the purpose of light-duty BEV testing were included in this study: the Urban Dynamometer Driving Schedule (UDDS, also known as the LA4) city cycle, the Highway Fuel Economy Test (HWFET) highway cycle, and the US06 aggressive driving cycle (one of the supplemental federal test procedure cycles). A sequence of these cycles was completed at each test temperature to provide a detailed view of the performance of each vehicle at different temperatures. The drive cycle traces were followed by test technicians who controlled the vehicle on the chassis dynamometer using a cycle trace display.

2.3. Short Multi-Cycle Test Plus Steady-State (SMCT+) Procedure

The version of the SAE J1634 procedure published in 2021 includes two alternative test procedures, both of which are intended to reduce the test burden on test facilities, specifically the Short Multi-Cycle Test (SMCT) and Short Multi-Cycle Test Plus Steady-State (SMCT+) procedures [23]. For this study, the SMCT+ procedure was chosen over the SMCT because it does not require the use of a bidirectional charger (BDC), which is used for battery depletion during the SMCT, as no BDC was available at the testing facility. The SMCT+ allows battery depletion to be performed on the chassis dynamometer at a constant speed of 65 mph (105 km/h). The SMCT+ offers test duration and test burden advantages over the original Multi-Cycle Test (MCT) procedure, as the MCT requires an additional constant speed cycle to be driven in the middle of the test sequence [23]. In summary, the SMCT+ was chosen for this program because it offers some of the test duration advantages of the SMCT, while allowing the test to proceed using only a chassis dynamometer, like the MCT.

Specifically, the SMCT+ procedure begins with a sequence of seven drive cycles: two repeats of the UDDS, one HWFET, one US06, a second HWFET, and a final two repeats of the UDDS [23], as shown in Figure 2, along with two 10–30 min key-off soak times to allow the test computers to be reset. Following this sequence (and another 10–30 min key-off soak), the vehicle is driven at a constant speed of 65 mph until the end-of-test criterion is met, meaning the battery is depleted. The end-of-test criterion specifies that the

vehicle should be decelerated smoothly to a stop within 15 seconds when it can no longer meet the desired speed, 65 mph (105 km/h), to within a 2 mph (3.2 km/h) tolerance [23]. This end-of-test criterion was followed for all full-depletion test (FDT) days.

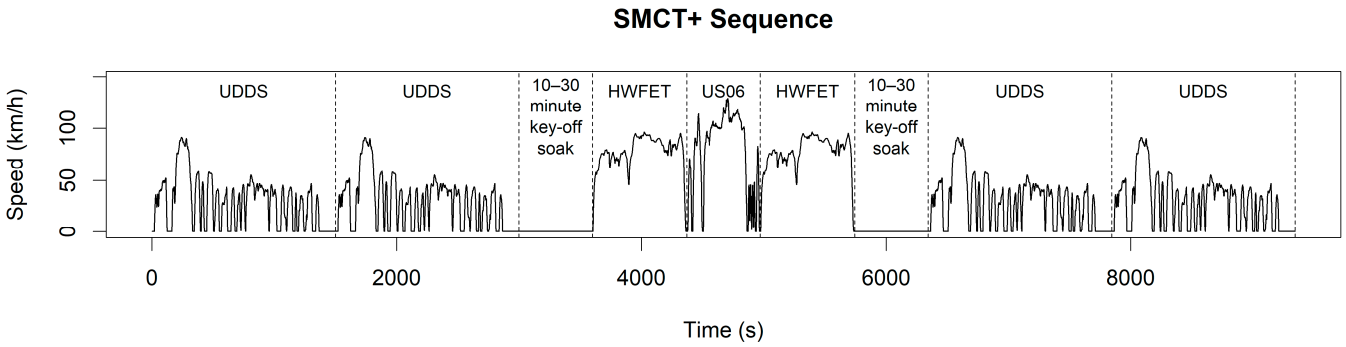

Figure 2. SMCT+ initial drive cycle sequence, including two UDDS repeats; one HWFET, US06, and HWFET sequence; and two additional UDDS repeats.

Some test days included only the seven initial drive cycles from the SMCT+ procedure, exactly as shown in Figure 2, and these were considered partial-depletion test (PDT) days. The results of these partial-depletion tests were used in the calculation of energy consumption (and driving range, by extension) but could not be included in the calculation of Usable Battery Energy (UBE) because the battery was not fully depleted.

2.4. Test Conditions and Cabin Conditioning

The intent of this study was to test the vehicles at different temperatures, thus obtaining energy consumption data for a variety of possible conditions. A temperature of 25 °C was set as the baseline temperature for testing, as this is the standard condition for laboratory testing of vehicles. For this condition, no heating or cabin conditioning of any sort was used. The cold temperatures used to compare to this baseline were 0 °C, −7 °C (the standard temperature for cold testing), and −10 °C. At each of these additional temperatures, the cabin conditioning was set to a 22 °C temperature setpoint with automatic fan speed and direction. The defrost setting was not used unless automatically initiated.

2.5. Test Sequence and Test Matrix

Certain test operations were followed in sequence, as shown in Figure 3. Testing for each week began with a preparatory "prep" cycle (partial depletion) followed by a full charge. Every test day, regardless of the type of test, began with the vehicle having a fully charged battery (as close to 100% State of Charge, or SOC, as the vehicle software would allow). This was achieved by charging the vehicle overnight after each prep and test. SMCT+ tests could be repeated without an additional prep cycle if the new cycle was run on the next calendar day, as shown in Figure 3.

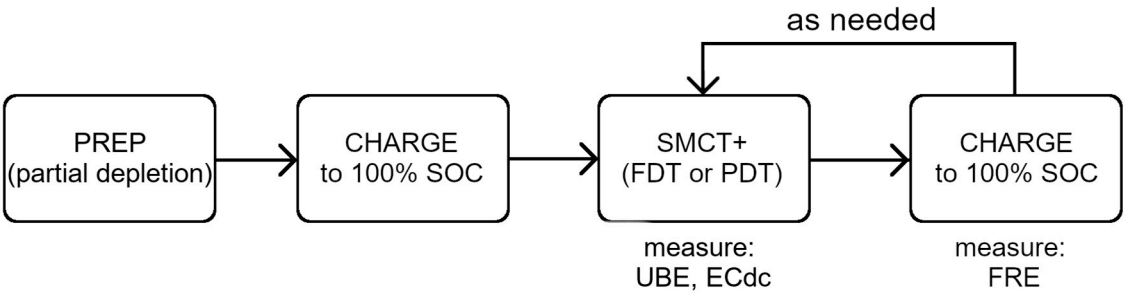

Figure 3. Testing sequence showing prep, charge, and SMCT+ operations.

This test program included full-depletion tests (FDTs) of the SMCT+ type, where the battery of the vehicle was fully depleted at the end of the test, as well as some partial-depletion tests (PDTs), where only the first seven cycles of the SMCT+ were driven, as shown in Table 2. Due to time constraints, the additional PDTs were only run at 25 °C and −7 °C, while FDTs were completed at each temperature. The same test matrix was followed for both test vehicles. Typically, the SAE J1634 SMCT+ procedure (whether partial or full depletion) is run only at the standard temperature (25 °C); however, in this study it was completed at cold temperatures as well to analyze the operation of the heating systems on the test vehicles.

Table 2. Test matrix (repeated for each vehicle).

Temperature	25 °C	0 °C	−7 °C	−10 °C
Full-Depletion Days	1	1	1	1
Partial-Depletion Days	2	0	2	0

2.6. Instrumentation

Vehicle #1 (PTC) was tested first for several weeks, and then Vehicle #2 (heat pump) was tested, since most of the instrumentation was shared between the two vehicles. The main instrumentation for this test program consisted of a pair of Hioki PW6001 power analyzers (Hioki E.E. Corporation, Nagano, Japan), connected and synchronized by fiber-optic cable, to form a 12-channel power analyzer system. The traction battery voltage signal was read directly from inside the battery "penthouse" (a compartment on top of the battery pack) and was used as the voltage signal for all high-voltage systems. The case of the penthouse was modified to allow the voltage leads to exit this compartment. Up to 11 Hioki current probes (depending on the number of vehicle sub-systems) were used to measure the current from each sub-system within the vehicle. The grid current and voltage of approximately 208V AC were also measured during charging, via a separate AC grid breakout box and current probe upstream of the Electric Vehicle Supply Equipment (EVSE). Table 3 includes a list of the sub-systems that were monitored and the power analyzer setup for each vehicle.

Some of the channels listed for each vehicle in Table 3 are repeated with positive and negative signs noted. This is due to the chosen method of instrumentation, which was designed to be as non-invasive to the vehicles as possible. Since the Hioki current probes (models CT6843 and CT6845-05) are of the clamp-on type, they were installed directly over top of the insulated current-carrying cables, without cutting into the wires. However, electric vehicle high-voltage system cables generally include shield wiring around current carriers, and the induced currents within these shield wires can cause significant inaccuracy in the measurements if they are not accounted for. A so-called "dual-probe" method was used to account for this.

The dual-probe method consists of installing two probes on the electrical cables supplying power to the system being measured, where one probe is clamped around the positive cable and another probe on the negative cable, in opposite directions. With these two probes measuring the current for the same system, the average value of the two current probe readings cancels out the induced shield currents travelling through the positive and negative shield wires. This method is only possible to use if each system in the drivetrain has its own positive and negative cabling (i.e., not a common negative), and they also include shield wires that are electrically connected to each other. The dual-probe method was used for most of the channels in Table 3; however, some Hioki channels did not use this method because their cabling was not shielded, specifically the low-voltage DC–DC output and the AC grid connection.

Table 3. Power analyzer instrumentation channels for each test vehicle.

Ch.	Vehicle 1 (PTC Heater)	Voltage Range (V)	Current Range (A)	Vehicle 2 (Heat Pump)	Voltage Range (V)	Current Range (A)
1	Front Motor (+)	600	500	Front Motor (+)	600	500
2	Front Motor (−)	600	500	Front Motor (−)	600	500
3	Rear Motor (+)	600	500	Rear Motor (+)	600	500
4	Rear Motor (−)	600	500	Rear Motor (−)	600	500
5	DC–DC Input/Main Battery (Charging) (+) [1]	600	20	DC–DC Input/Main Battery (Charging) (+)	600	20/40 (changed)
6	DC–DC Input/Main Battery (Charging) (−) [1]	600	20	DC–DC Input/Main Battery (Charging) (−)	600	20/40 (changed)
7	A/C Compressor (+)	600	80	-	-	-
8	A/C Compressor (−)	600	80	-	-	-
9	PTC Heater (+)	600	80	Heat Pump (+)	600	80
10	PTC Heater (−)	600	80	Heat Pump (−)	600	80
11	DC-DC Output	15	200	DC–DC Output	15	200
12	Dyno Speed/AC Grid (Charging) [1]	15/300 (DC/AC)	-/80	Dyno Speed/AC Grid (Charging)	15/300 (DC/AC)	-/80

[1] The "DC–DC Input/Main Battery" and "Dyno Speed/AC Grid (Charging)" channel names are split to denote the fact that they collected different data during driving and charging, and the parameters for these channels are split in the same way.

2.7. Test Vehicle Road Load Derivation

The test vehicles chosen for this program were of different model years, leading to small variations in the target road load coefficients reported by the manufacturer and the set coefficients derived on the chassis dynamometer. The target road load coefficients were determined by the manufacturer and are reported to the United States Environmental Protection Agency (EPA), which makes them publicly accessible on their website [30]. Using these publicly available "target" coefficients, "set" coastdown coefficients were determined at 25 °C for each vehicle on the AWD chassis dynamometer at TEEL via the SAE J2264 procedure [31]. Additionally, the cold temperature target coefficient values were increased by a value of 10%, and new set coefficients were then determined (via coastdowns at −7 °C for all cold temperatures). This 10% increase in target coefficient values is part of standard chassis dynamometer testing at cold temperatures and is intended to account for increased wind resistance and rolling resistance on the vehicle at cold temperatures but does not affect the heating system operation of the vehicle. The appropriate set coefficients for each vehicle and condition were used for dynamometer road load simulation during all chassis dynamometer testing (including both standard drive cycles and constant speed cycles). The target and coastdown coefficients for Vehicle 1 and Vehicle 2 are available in Table 4 and Table 5, respectively.

Table 4. Vehicle 1 (PTC heater) target and set dynamometer coefficients.

Vehicle 1: 2020 Tesla Model 3 Long Range AWD				
Coefficient Type	Target (Standard)	Set (Standard)	Target (Cold)	Set (Cold)
Temperature	25 °C	25 °C	0 °C, −7 °C, −10 °C	0 °C, −7 °C, −10 °C
A [hp@50mph]	5.16	−0.01	5.68	−0.63
B [hp@50mph]	0.20	−0.15	0.22	−0.66
C [hp@50mph]	5.00	4.49	5.50	4.95
Total [hp@50mph]	10.36	4.33	11.40	3.66

Table 5. Vehicle 2 (heat pump) target and set dynamometer coefficients.

Vehicle 2: 2022 Tesla Model 3 Long Range AWD				
Coefficient Type	**Target (Standard)**	**Set (Standard)**	**Target (Cold)**	**Set (Cold)**
Temperature	25 °C	25 °C	0 °C, −7 °C, −10 °C	0 °C, −7 °C, −10 °C
A [hp@50mph]	4.66	0.10	5.13	−1.44
B [hp@50mph]	0.58	−0.04	0.64	−0.37
C [hp@50mph]	4.93	4.53	5.42	4.96
Total [hp@50mph]	10.17	4.59	11.19	3.15

The target coastdown coefficients were used to calculate the expected road load on the vehicle at any speed, as shown in Figure 4. As expected due to their similar design and target coefficient totals, both vehicles show very similar road load characteristics. Figure 4 also shows the curves generated by the set coefficients (those used by the dynamometer to simulate the road load curves at the vehicle's wheels). Again, these are similar between the two vehicles, illustrating that the magnitudes of the vehicles' drivetrain power losses were similar.

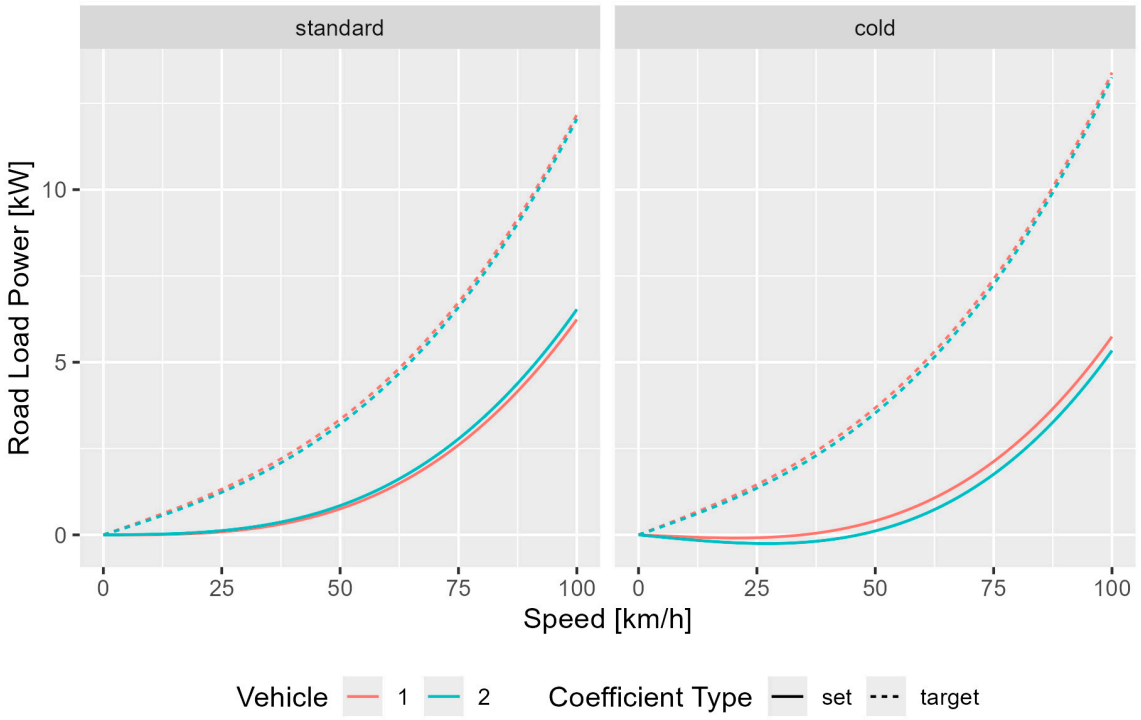

Figure 4. Road load power versus vehicle speed, based on target and set coastdown coefficients.

2.8. Calculations

2.8.1. Energy Consumption

Component energy was measured and reported by the Hioki power analyzers during each drive cycle driven on the chassis dynamometer. The DC energy sent from the battery to each component was added together to make a total DC battery energy value in Watt-hours (Wh) for each test (denoted as E_{DC}). The DC energy consumption (EC_{DC}) in Wh/km was calculated by dividing this value by the distance driven (D) in km for the corresponding test, as shown in Equation (1).

$$EC_{DC} = \frac{E_{DC}}{D} \quad (1)$$

2.8.2. J1634 Combined Energy Consumption Calculation

The SAE J1634 Recommended Practice includes calculations to combine the results from each individual drive cycle during an SMCT+ test day into a composite energy consumption value for each cycle type (i.e., for the UDDS, HWFET, and US06 cycles) using "phase-scaling factors" (denoted as "k" in equations) [23]. This allows the cold-start effect, present in the first test of any daily test sequence, to be accurately represented and makes the UDDS energy consumption and range results more comparable to those of the other cycles which do not have this cold-start effect. The calculations for the UDDS cycle energy consumption in Wh/km are shown in Equation (2). For the HWFET and US06 cycles, the phase-scaling factors (k) equal one divided by the number of cycles of each type, so their final EC_{DC} values are equivalent to taking that cycle's average energy consumption for the test day (for US06, there is only one test cycle, so the value for that one is taken as the final daily value).

$$EC_{DC\ UDDS} = \sum_{i=1}^{4} \left(k_i \times EC_{DC\ UDDS_i}\right)$$
$$\text{where } k_1 = \frac{E_{DC\ UDDS_1}}{E_{DC_{Total}}} \quad (2)$$
$$\text{and } k_{2,3,4} = \frac{1 - k_1}{3}$$

2.8.3. Driving Range Estimation

The Usable Battery Energy (UBE) in Wh was calculated by taking the summation of all the total DC battery energy (E_{DC}) values for each drive cycle on a particular day. Only one full-depletion test was completed at each temperature for each vehicle to obtain this UBE. Then, to obtain the estimated driving range in km for a particular cycle, this UBE in Wh was divided by the cycle-specific combined DC energy consumption ($EC_{DC\ cycle}$) in Wh/km, as shown in Equation (3).

$$\text{Range}_{calc} = \frac{UBE}{\text{EC}_{\text{DC cycle}}} \quad (3)$$

3. Results

3.1. Drive Cycle Metrics

To ensure that neither vehicle obtained an advantage due to discrepancies in following the driving trace, selected average statistics comparing each vehicle's driven trace over each type of cycle are shown in Table 6. The distance varied only for the CSC65 cycle, as the length of this cycle depends on the battery capacity and energy consumption of each vehicle. Otherwise, the distance, kinetic intensity, average driving speed (not including stops), and average acceleration rates were very similar between cycles. The kinetic intensity is of particular interest when comparing the cycles driven between vehicles, as this measurement is a composite value that attempts to quantify the "aggressiveness" of a drive cycle [32], and the results show that the kinetic intensities were very similar between the two vehicles' tests.

Table 6. Average drive cycle statistics during testing.

Cycle Type	Vehicle	Average Cycle Distance [km]	Average Kinetic Intensity [1/km]	Average Driving Speed [km/h]	Average Accel. [m/s^2]	Average Decel. [m/s^2]
CSC65	1	325.3	0.01	104.8	0.02	−0.01
CSC65	2	393.5	0.01	105.1	0.01	−0.01
HWFET	1	16.6	0.14	78.2	0.17	−0.19

Table 6. *Cont.*

Cycle Type	Vehicle	Average Cycle Distance [km]	Average Kinetic Intensity [1/km]	Average Driving Speed [km/h]	Average Accel. [m/s^2]	Average Decel. [m/s^2]
HWFET	2	16.6	0.14	78.2	0.17	−0.19
UDDS	1	12.0	0.79	36.6	0.44	−0.49
UDDS	2	12.0	0.78	36.8	0.44	−0.48
US06	1	12.9	0.24	81.1	0.60	−0.59
US06	2	12.9	0.25	81.8	0.61	−0.60

3.2. Average Heating System Loads

One way to analyze the heating system performance of the test vehicles is to compare the average load required by the heating system of each vehicle. Looking at the power, or load, demanded by each system rather than its energy consumption removes the effect of the selected drive cycle trace on heating system performance and allows for a comparison between heating loads during disparate cycles and over the course of the full test day. The average heating system loads during each of the drive cycles performed by each vehicle on each test day are illustrated in Figure 5 (note that the 25 °C temperature results are not relevant in this scenario because the heating systems were turned off at this ambient temperature). The cycles in Figure 5 are separated by their driven order during the day and are denoted using two numbers referring to their "round" and "mode". "Round" refers to each sequence of tests that were loaded into the test computer (for example, round 1 consists of two repeats of the UDDS cycle in quick succession). "Mode" refers to the drive cycle's order within its round; for example, "1-2 UDDS" refers to mode 2 of round 1, the second cycle of the first round of testing and the second cycle driven overall.

For both vehicles, the average heating system load was highest in the first (cold-start) cycle of the test day, as the vehicles were soaked overnight at the ambient test temperature and the heating systems had to increase the cabin temperature significantly to reach the 22 °C setpoint. Subsequent tests showed lower heating loads as the cabin was already partially or fully warmed up prior to the start of these cycles because of heater use during the preceding tests. Pre-heating the vehicles could mitigate some of the cold-start effect on the heating system load (and therefore could improve energy consumption and driving range as well); however, pre-heating was not included in this test program.

The heat pump-equipped vehicle (Vehicle 2) generally recorded lower average heating system loads than the PTC heater-equipped vehicle (Vehicle 1), except on cold-start at the coldest conditions (−10 °C and −7 °C). At −10 °C, Vehicle 2 had a higher heating system load than Vehicle 1 for the first two test cycles of the day. At −7 °C, the heating system loads were similar for both vehicles on the first test of the day. For all other tests, Vehicle 2 had lower average heating system loads than Vehicle 1. The reason for this reversal of heating load at very cold temperatures could be due to "lossy mode" operation of the heat pump, where it creates heat directly by running the compressor inefficiently, as opposed to efficiently scavenging heat from the surroundings and transferring it to the cabin [21,22]. In this lossy mode, the energy use of the heat pump appears to have been greater than that of the simple PTC heater, perhaps due to the additional steps required to transfer the heat first through the refrigerant and then to the cabin (instead of directly heating the cabin intake air like the PTC) [22]. An additional function of the heat pump system (which is not present in the PTC heater system) is that it can also help heat the vehicle battery as needed [22], which may account for part of this larger load at cold temperatures as well.

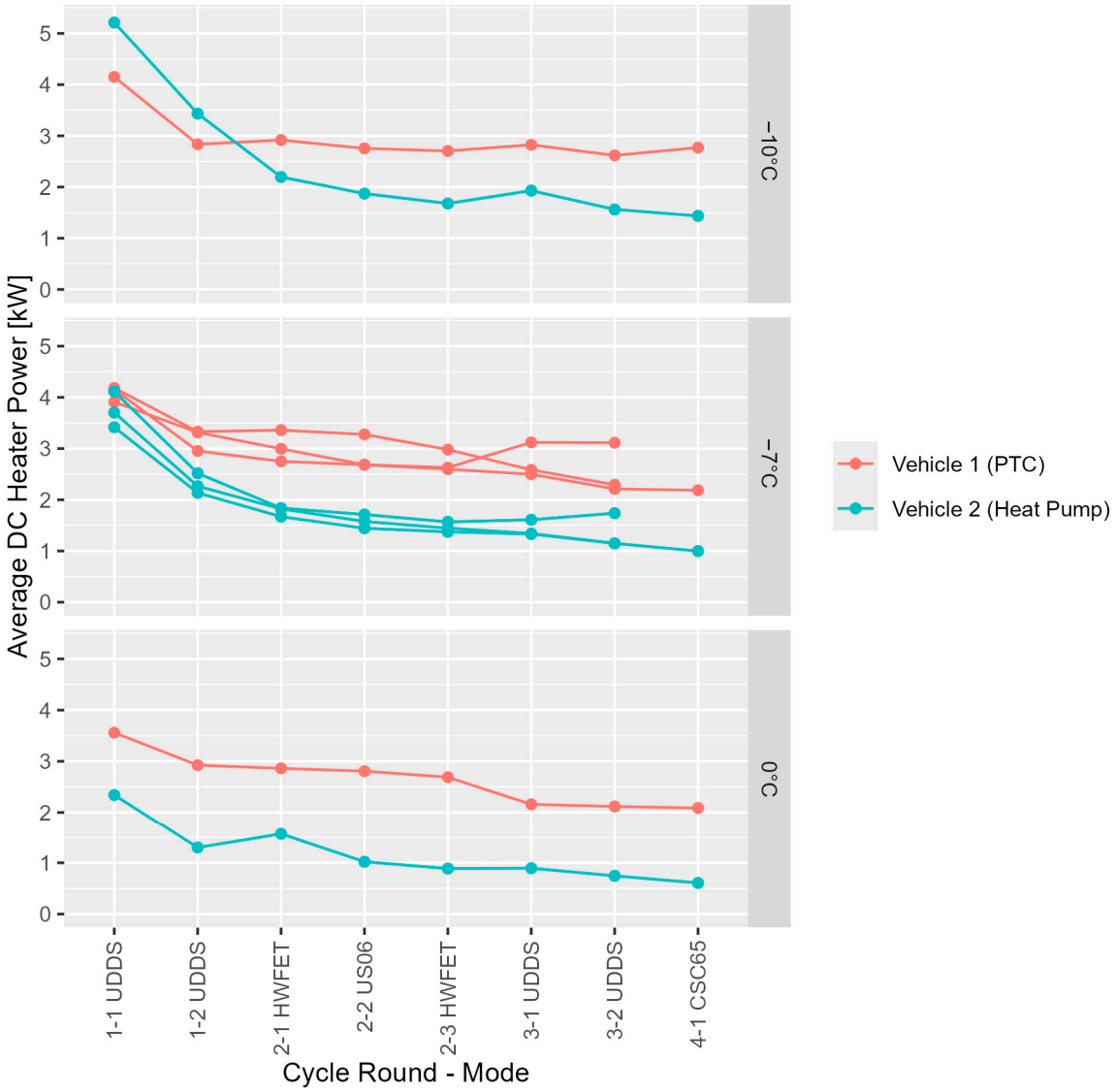

Figure 5. Average heating system loads at different temperatures for each vehicle and test type/day by sequence order.

Comparing all test days, the heat pump showed the greatest efficiency advantage over the PTC heater at a moderately cold temperature of 0 °C, using less than half the average power of the PTC heater on many cycles at that temperature. At −7 °C and −10 °C, the heat pump advantage was low (and, as mentioned, became a disadvantage at −10 °C upon cold-start), but improved as the test days progressed. Over longer drives at these temperatures, this advantage would be helpful to increase the vehicle's driving range once the cabin reached its setpoint temperature.

3.3. Instantaneous Heating System Power

The instantaneous heating system power throughout each cycle was captured from each vehicle on each cold temperature test day. This instantaneous loading is shown in Figures 6 and 7. As denoted in Figure 5, the heating loads are higher at cold temperatures and on cold-start (the first cycle of the day). However, Figures 6 and 7 show the additional second-by-second variation in heating load over the course of each test.

Figures 6 and 7 show that Vehicle 1, in red, had large variations in heating load that fluctuated very quickly. This is typical of PTC-type resistive heater operation using a Pulse-Width Modulation (PWM) control system. On the other hand, the heat pump loads

are more consistent, with some cycling up and down evident in later test cycles during the day, but at a much lower frequency than the cycling of the PTC heater.

The cold-start peak power of the heat pump system in −10 °C conditions, at almost 8.75 kW, was higher than that of the PTC heater in the same conditions. At −7 °C, both systems showed similar power loads over the course of the cold-start cycle, but at 0 °C the heat pump showed a clear advantage throughout the cold-start test cycle. By the second test cycle of the day at −7 °C and at 0 °C, the heat pump was consistently using less power than the PTC heater system. By the third test cycle at −10 °C, the heat pump was again showing an advantage in lowering the heating system power.

Just before halfway through the first test cycle at −10 °C (1-1 UDDS), the heat pump load underwent a step change downward, indicating a change in operation which could coincide with a change from using "lossy mode" to using its regular "efficient" heat pump mode.

At the top of each segment of Figure 6, the "round" and "mode" of each cycle is shown. There was a 10-to-30 min break between each round of the test day. This explains the slight increase in heating load at the start of round 2 (the third cycle of the day).

Focusing on Figure 7, a similar effect is visible at the start of round 3, with a slight increase in heating system load for the heat pump-equipped vehicle in particular at all test temperatures. Otherwise, the heating system loads over the cycles in Figure 7 are relatively consistent, indicating that the cabin setpoint temperature had been achieved, and the systems were running in a steady-state manner to maintain cabin temperature rather than to increase it.

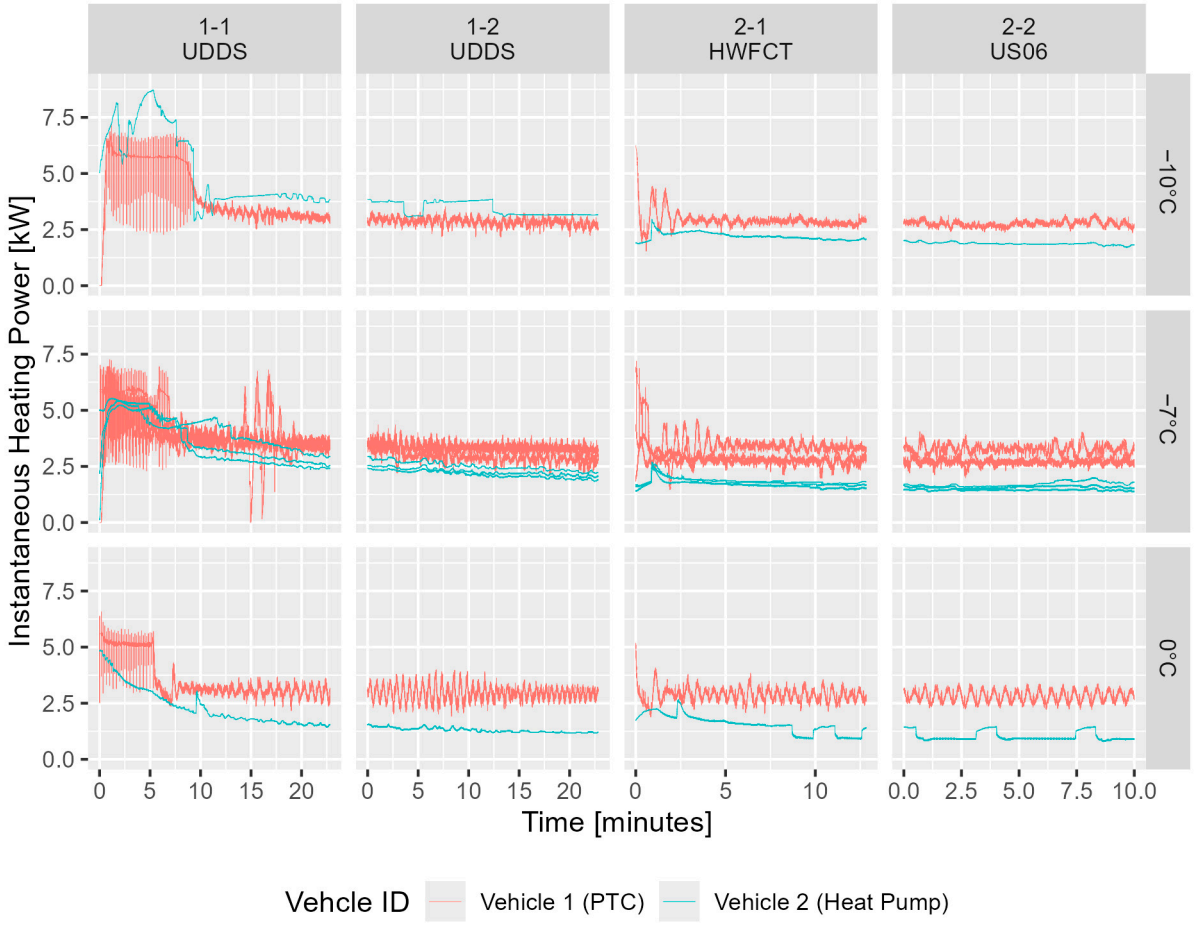

Figure 6. Instantaneous thermal management system power by cycle and temperature for both vehicles over the first four test cycles of each day.

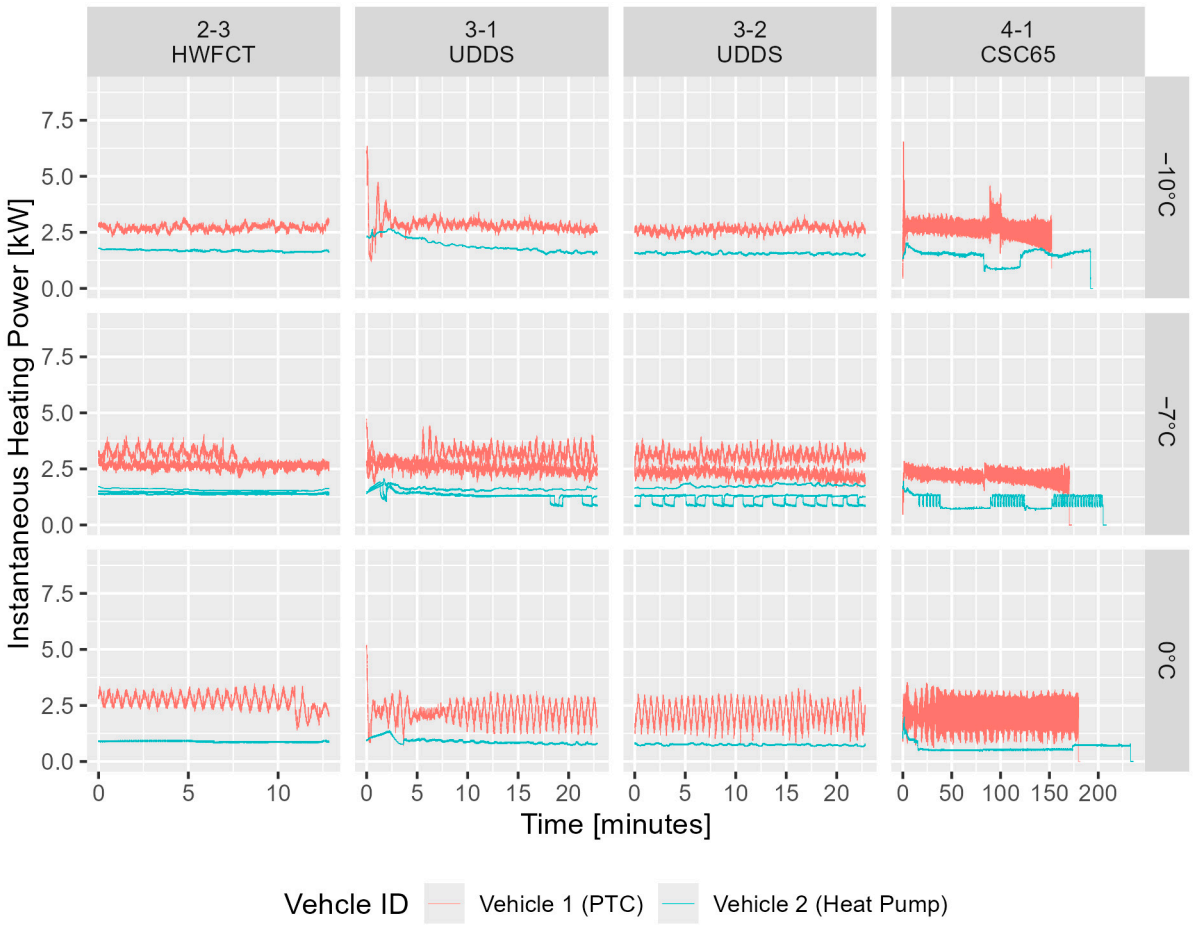

Figure 7. Instantaneous cabin thermal management power by cycle and temperature for both vehicles over the final four test cycles of each day.

Figure 7 shows the final test cycle of each day (4-1 CSC65), which was the constant-speed 65 mph depletion cycle. As shown on the *x*-axis of the graphs of this test cycle, the time taken to complete this depletion was significantly longer than that of the other individual cycles. Again, however, loading was relatively consistent during this cycle, with slight cycling of both systems evident (albeit with the PTC heater again generally cycling between loadings at a much higher frequency than the heat pump).

3.4. Component-Level Energy Consumption

Since each high-voltage component or system on the vehicles was measured independently, the energy consumption of each vehicle can be broken down as component-level energy consumption, as shown in Figure 8 (for ambient temperatures of −10 °C and −7 °C) and Figure 9 (for 0 °C and 25 °C). The total height of each bar in these figures represents the total energy consumption for the vehicle at that test condition (temperature and test cycle). Each bar is further broken down into motor/inverter energy consumption in its bottom section, accessory (DC–DC converter) energy consumption in its middle section, and heating system energy consumption in its top section (the heating system portion includes A/C compressor energy consumption used for dehumidification when applicable on Vehicle 1). Test conditions for which multiple repeats were conducted are represented by their average values (multiple tests were conducted for temperatures of 25 °C and −7 °C only). Each test cycle is shown in its chronological sequence during the test day with numbering pertaining to its "round" and "mode".

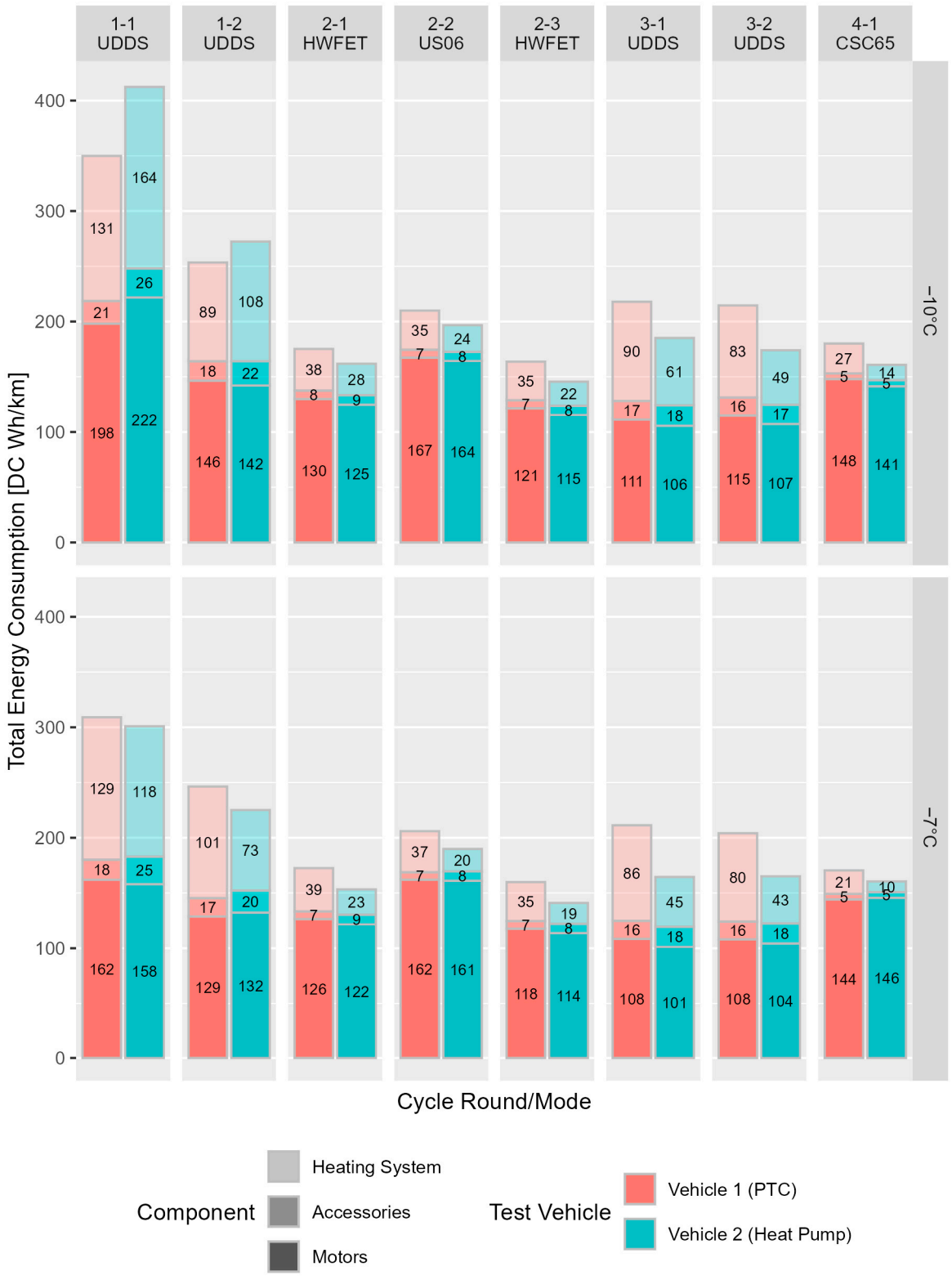

Figure 8. Energy consumption in Wh/km by cycle, round/mode, temperature, vehicle, and component (−10 °C and −7 °C).

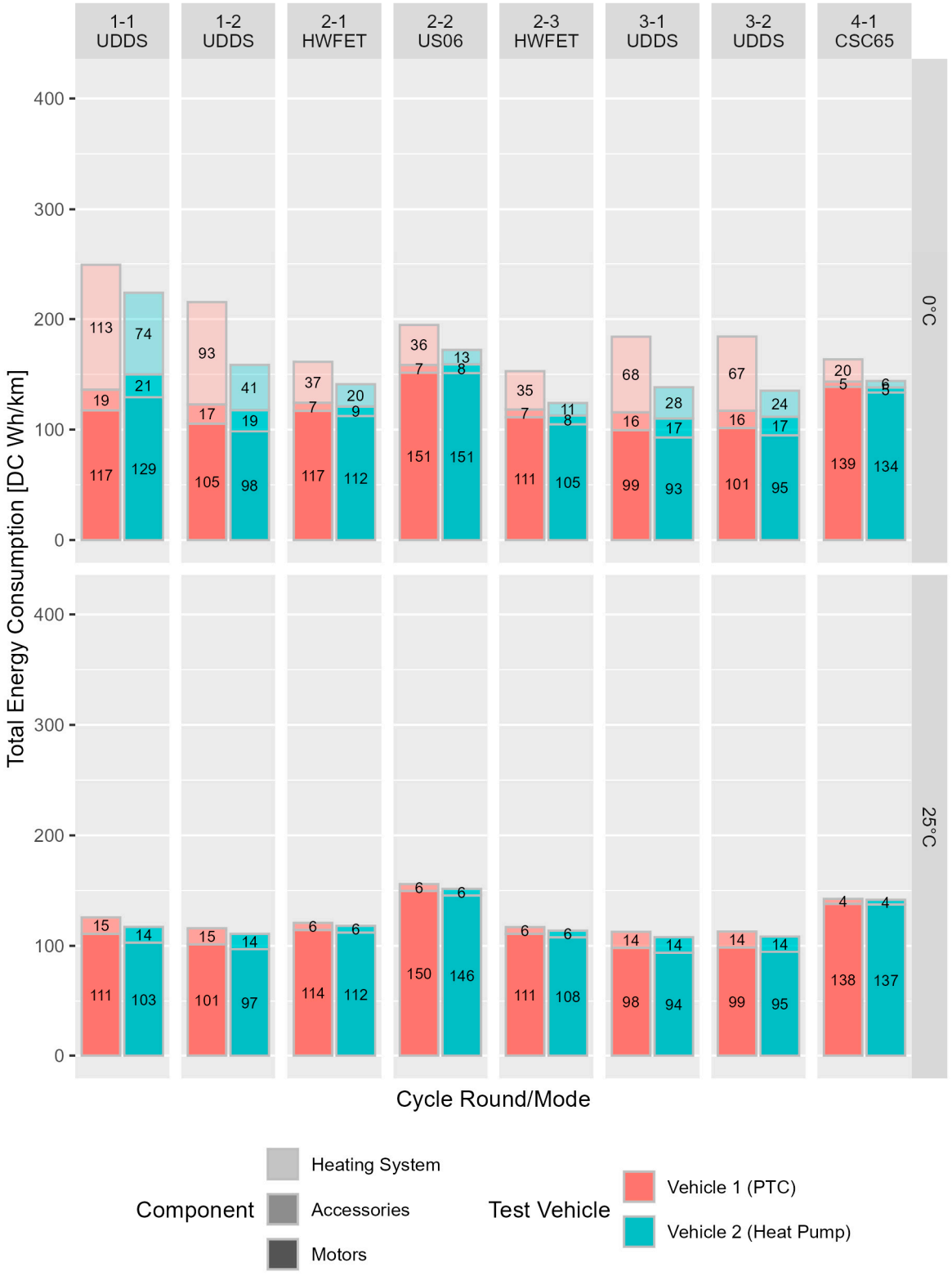

Figure 9. Energy consumption in Wh/km by cycle, round/mode, temperature, vehicle, and component (0 °C and 25 °C).

Similarly to the heating system loads shown in Figures 5–7, the heating system energy consumption values shown in Figures 8 and 9 were significantly higher during the first drive cycle of each day (cold-start) than in subsequent cycles and were sometimes high for the second drive cycle of the day as well. However, the effect of the driving cycle is also apparent in Figures 8 and 9: even though the heating loads of different test cycle

types (after the cold-start) may be similar in Figure 5, the effect of the heating load on energy consumption varied due to the test cycle. Generally, the effect of heating loads on cycles with higher average speeds (HWFET, US06, and CSC cycles) is lower than on the city-type cycle with lower average speeds (UDDS). This is because over a similar test duration, heating energy will be divided by a larger distance in the energy consumption calculation if the average vehicle speed was higher, leading to a lower energy consumption value for a similar heating load. This effect also means that the calculated vehicle ranges over the higher speed cycles are less affected by heating loads than those over the UDDS cycle, regardless of heating system, which is evident in the results in Sections 3.7 and 3.8 of this report.

Accessory energy consumption (which was measured at the input of the DC–DC converter) was affected by drive cycle speed in the same way as heating energy consumption. In general, however, the accessory energy consumption was much lower in magnitude than the heating energy consumption, as shown in Figures 8 and 9 (except during 25 °C testing, which had no heating component). Accessory energy consumption also did not vary as significantly due to temperature or cold-start conditions. The lowest accessory energy consumption was recorded during 25 °C testing, potentially due to the lack of cabin heating fan usage because cabin conditioning was turned off at this temperature.

The motor/inverter energy consumption shown in Figures 8 and 9 also varied significantly due to the cold-start condition, temperature, and cycle type. A portion of the motor/inverter energy consumed on cold-start may have been used to heat the vehicles' batteries during cold temperatures. The ability to use the motor/inverter system to provide heat for the battery is a feature of this vehicle model [21,22], and, unfortunately, the motor/inverter energy used to heat the battery could not be consistently broken out from the overall motor/inverter energy consumption. Cold temperatures also generally increase tire and drivetrain losses in vehicles, and this accounts for some of the increased motor/inverter energy consumption (especially at the coldest two temperature conditions).

The lowest outright motor/inverter energy consumption was recorded over the UDDS cycle, which features light acceleration rates and low average speeds, along with lots of opportunity for regenerative braking during deceleration. The highway (HWFET) cycle also had relatively low motor/inverter energy consumption due to its moderate speeds and lack of heavy acceleration. The US06 cycle (aggressive driving) had the highest motor/inverter energy consumption, except at cold temperatures where cold-start effects, such as cold tires, drivetrains, and battery heating, dominated during the cold-start UDDS cycles (as mentioned, this high energy consumption may be partly attributed in this case to the motor/inverter being used to heat the battery).

A quick estimate of the Coefficient of Performance of the heat pump system in each test condition (temperature, cycle, round, and mode) can be obtained by dividing the heating component of energy consumption of Vehicle 1 by that of Vehicle 2. This quick method assumes that the cabin heating energy required for both vehicles was identical under the same conditions, and that all the energy used by Vehicle 1's heating system went directly to heating the cabin. Using this method, the resulting COP of the heat pump system varied from 0.80 to 1.93 at −10 °C, from 1.09 to 2.10 at −7 °C, and from 1.53 to 3.33 at 0 °C. This illustrates the reduced advantage of the heat pump system at colder temperatures and in cold-start conditions (when it is suspected to have been using its lossy mode of operation).

3.5. DC Energy Consumption by Drive Cycle

The SAE J1634 Recommended Practice for testing BEVs includes calculations to convert the energy consumption over individual test cycles driven during the SMCT+ test sequence into composite values for each type of drive cycle (UDDS, HWFET, and US06) [23]. This

requires the use of a "Phase Scaling Factor", which lowers the cold-start effect on UDDS energy consumption, as explained in Section 2.8.2. The composite results for the HWFET and US06 test cycles are essentially the average values for each of those cycle types during each day. Figure 10 shows the J1634-calculated combined DC energy consumption values for each vehicle, test temperature, and drive cycle type (except for the CSC, as it is not a standard compliance cycle). Typically, the SAE J1634 SMCT+ procedure is run only at standard temperature (25°C); however, the same calculations have been adapted to use at cold temperatures in this study to analyze the cold temperature operation of the vehicles. The DC energy consumption values listed in Figure 10 are used later in this paper along with the measured UBE to calculate the expected driving ranges.

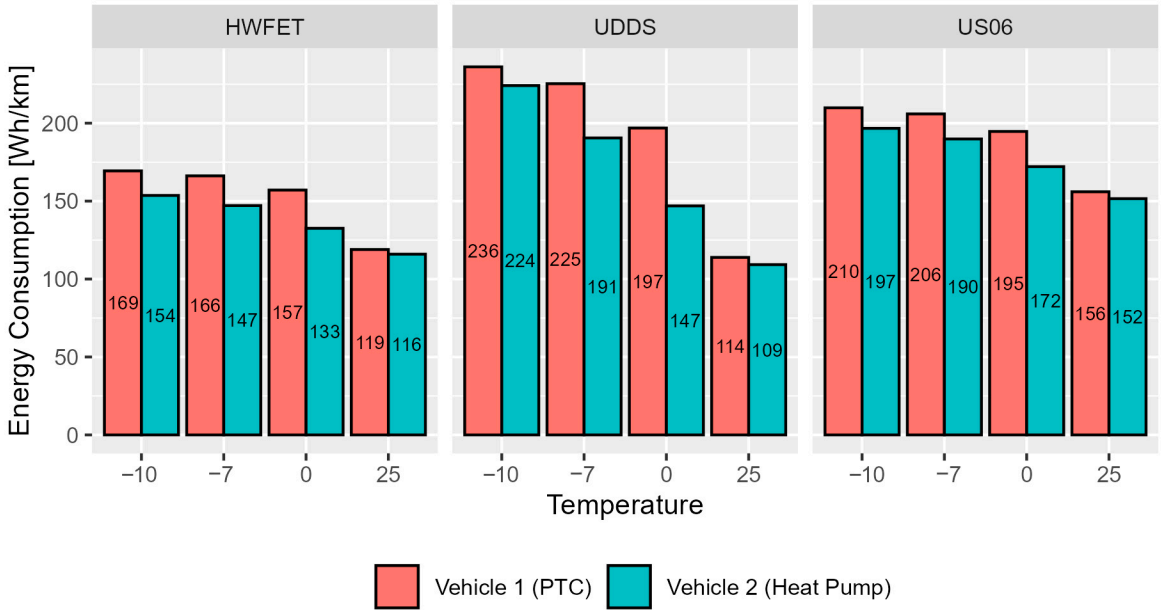

Figure 10. SAE J1634-style combined DC energy consumption by drive cycle and temperature for each vehicle.

Figure 10 shows that the largest temperature effects on energy consumption occurred during the UDDS cycle, with the UDDS energy consumptions at −10 °C for both vehicles being over twice that of their respective UDDS energy consumptions at 25 °C. As mentioned in previous sections, this large increase in energy consumption is due to a combination of cold-start effects on the heating and drivetrain systems, increased heating loads at cold temperatures, and the low average speed of the UDDS cycle which spreads the energy used over a shorter distance when calculating energy consumption. Since these EC_{DC} values are weighted averages and cold-start effects are therefore reduced, the heat pump-equipped vehicle (Vehicle #2) managed to obtain lower energy consumption than Vehicle #1 over all composite cycle results and temperatures (even though it had higher energy consumption over the first two UDDS cycles at −10 °C, as shown in Figure 8, this was overcome by its advantage during the other two UDDS cycles at that temperature). The improved energy consumption due to the heat pump was most apparent at 0 °C in the UDDS and HWFET cycle results. The improvement in efficiency for Vehicle #2 is also obvious at −7 °C in the UDDS cycle results and at 0 °C in the US06 cycle results, among other conditions.

3.6. Usable Battery Energy

Figure 11 shows the recorded UBE for each completed full-depletion test at each temperature and for each test vehicle. As shown in Table 1, the UBE for Vehicle #1 was expected to be slightly lower than that of Vehicle #2. At 25 °C, however, neither vehicle

reached its UBE reported during certification at this temperature (potentially due to battery degradation prior to testing). The UBE of electric vehicles is generally reduced at low temperatures due to temperature effects on Li-ion batteries [33]. This was true for both test vehicles in this study, with their highest UBE values being recorded at 25 °C. Uncharacteristically, the lowest UBE for Vehicle #2 was recorded at a moderate 0 °C, and the UBE at −7 °C was higher than the UBE at 0 °C for both test vehicles. This may partly be explained by inter-test variability, as the UBE was recorded only once at each test temperature for each vehicle (8 full-depletion tests in total).

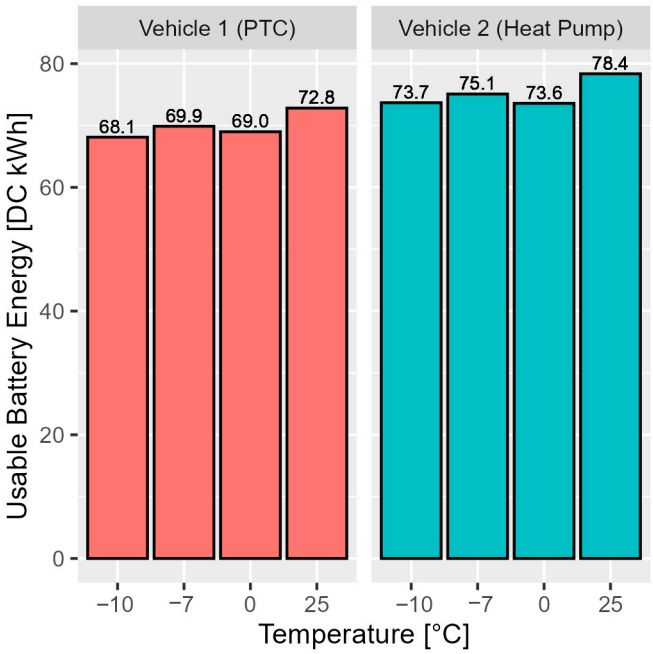

Figure 11. Usable battery energy of both test vehicles during full-depletion tests at different temperatures.

The UBE values shown in Figure 11 were used as part of the calculation of the vehicles' ranges over the test cycles at different temperatures. The reduced UBE and increased energy consumption at cold temperatures affected the results in both Sections 3.7 and 3.8.

3.7. Calculated Driving Range by Drive Cycle

Using the methods described in Section 2.8.3, the authors determined an estimated driving range for each test cycle at each test temperature, as shown in Figure 12. Combining both the UBE and the DC energy consumption values from previous sections, the driving range for each cycle type and temperature was calculated for both vehicles. Since Vehicle #2 has a slightly larger battery capacity than Vehicle #1, its range was consistently higher than that of Vehicle #1. However, the intent of this study is to characterize the effect of heating systems on vehicle energy consumption and range, so the differences in range between temperature conditions for each vehicle, and not their absolute values, are the key takeaways from Figure 12.

The results shown in Figure 12 reveal significant range reductions for both vehicles at cold temperatures, especially over the UDDS cycle. The UDDS cycle range is particularly affected by heating in cold temperatures because of its low average speed, which results in higher heating energy consumption per unit distance than "faster" drive cycles and a more than 50% reduction in driving range at the coldest temperature when compared to 25 °C. Conversely, the maximum range of each vehicle was achieved over the UDDS cycle at 25 °C, since this cycle has relatively gentle accelerations and has low average speeds (leading to low aerodynamic drag losses and low drivetrain energy consumption).

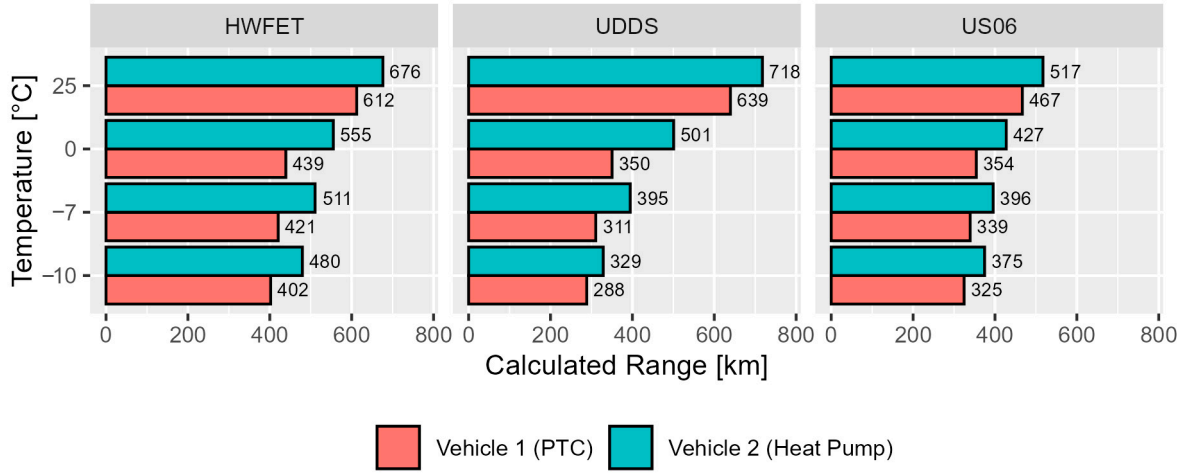

Figure 12. Calculated vehicle range for each cycle and temperature, with J1634 phase-scaling factors applied.

The US06 drive cycle resulted in the lowest calculated range for both vehicles at 25 °C, owing to its aggressive accelerations and high-speed driving. However, at the coldest temperatures both vehicles achieved a higher calculated range on the US06 cycle than on the UDDS cycle, due in part to the less pronounced effect of heating system usage over a higher speed cycle. The HWFET tests had the longest ranges for both vehicles at any temperature, except for 25 °C, since heating energy consumption values were low due to the high average speeds of this cycle, and because the HWFET driving cycle is more moderate in both speeds and acceleration rates than the US06 cycle.

The next section shows a method to directly compare the two vehicles and their heating systems using the percentage of range retained rather than the absolute calculated range of each vehicle.

3.8. Percentage Range Retained in Cold Temperatures

It is informative to look at the range retained as a percentage of the maximum range for each cycle and vehicle, as illustrated in Figure 13. This type of normalization allows for a direct comparison of the ranges retained at different temperatures over different cycles between the two vehicles (and their heating strategies). In this graph, each bar represents the associated vehicle's calculated range at different temperatures, as a percentage of its own maximum range over that cycle at 25 °C. This is an attempt to remove the effect of the differences in maximum battery capacity and motor output, and other discrepancies between the vehicles while still accounting for any range reductions due to test conditions and heating system efficiency. These differences between model years may still have affected the results slightly, but their effect could not be quantified.

Figure 13 reveals that the improved range retention capability of Vehicle 2 (heat pump) is highest at 0 °C, increasing the percentage of the retained range by 15% over Vehicle 1 (PTC heater) on the UDDS cycle, 10% on the HWFET cycle, and 7% on the US06 cycle at this temperature. At the two coldest temperatures, the range retention of Vehicle 2 is between 1% and 5% greater than that of Vehicle 1. The average range retention improvement in Vehicle 2 over Vehicle 1 was 7% over the UDDS, 7% over the HWFET, and 4% over the US06 cycles over all cold temperatures combined. This level of improvement in range retention is modest but still significant for electric vehicle users in cold climates, where range loss in the cold can be a significant barrier to BEV adoption. Whether adding a heat pump system is a justifiable upgrade to a vehicle depends on the cost of the system, customer requirements for winter driving, and marketability. In colder climates like in Canada, many

new BEVs are now either equipped with a heat pump as standard equipment or have one as an optional range-extending heating system for cold weather.

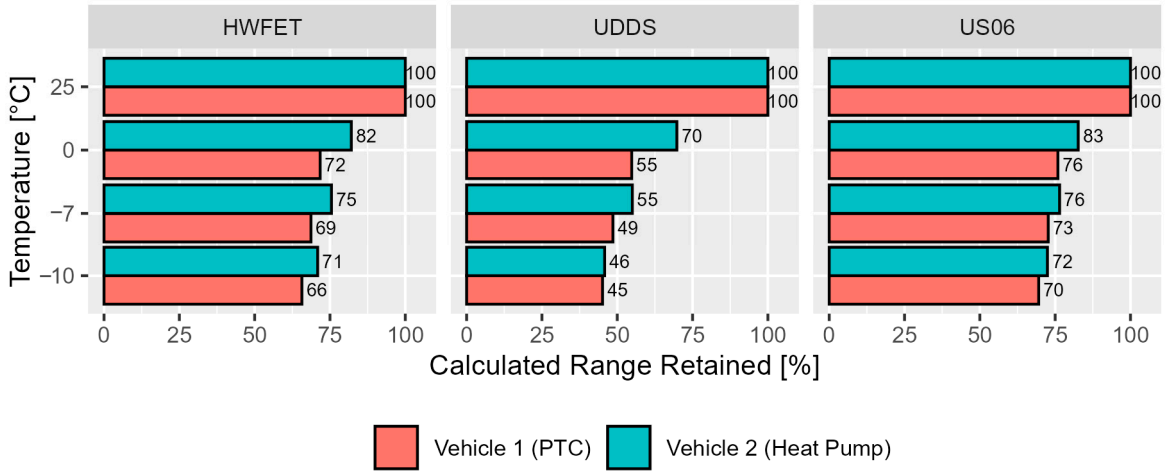

Figure 13. Estimated driving range percentage retained over different cycles at different temperatures, by vehicle, with J1634 phase-scaling factors applied; normalized to the highest range value for each vehicle and cycle.

4. Discussion

4.1. Energy Consumption and Range Retention

Vehicle 2 (heat pump) generally achieved lower heating energy consumption and better range retention at low temperatures than Vehicle 1 (PTC heater). However, certain conditions (cold-start at −10 °C) favoured the PTC heater. Heat pumps using R1234yf, such as the one tested in this study, generally show reduced performance at lower temperatures (in terms of both heating capacity and COP) [34] and may not be able to operate effectively at very cold temperatures without the assistance of a supplementary heater (usually a PTC heater). This explains the reduction in Vehicle 2's energy consumption and range retention advantages as the test temperatures were reduced.

Testing at temperatures colder than −10 °C was not possible at this facility but would be of interest since Canadian weather conditions can reach lower temperatures. This vehicle's implementation of a heat pump solution did not include a backup PTC heater for extremely cold temperatures (likely due to the additional cost), whereas many BEVs do include a PTC heater in addition to a heat pump. A backup PTC heater may have helped improve Vehicle 2's performance at the coldest temperatures, when its heating system was less efficient.

Pre-heating the cabin while plugged in to the AC grid and prior to driving each vehicle would lead to reduced heating energy demand over the cold-start cycles, decreasing energy consumption and thus increasing the driving range. This test scenario was not included in the design of this study but could be used as a strategy for increasing the cold-weather BEV range in the real world. Pre-heating may also increase the range retention advantage of a heat pump-equipped vehicle, since it would remove much of the cold-start effects at the conditions where the heat pump was at a disadvantage (cold-start at very cold temperatures).

4.2. Alternative Cabin Heating Solutions

Alternative cabin heating solutions have also been proposed for the BEV market, but none have been widely commercialized. Phase-change materials and radiant heating solutions have been proposed by researchers and manufacturers [35,36]. Alternative

refrigerants have also been proposed for use in electric vehicle heat pump systems, such as carbon dioxide (CO_2), known in the industry as R744, and propane, known as R290. Using a carbon dioxide refrigerant in heat pump systems has been shown to improve heating performance (including COP) at very cold temperatures (with a potential reduction in efficiency for cooling) [37]. Another benefit of both CO_2 and propane as refrigerants is that they do not contain persistent chemicals, since R1234yf, which is currently widely used in the automotive industry, is suspected by some to be a source of persistent chemicals [38].

4.3. Charging Infrastructure

In the long term, additional charging infrastructure may alleviate some of the importance of maintaining maximum driving range at cold temperatures. However, the efficiency benefits of heat pump systems from an electricity use and greenhouse gas (GHG) perspective will continue to be important, because they can reduce strain on the electricity grid and reduce GHG emissions, even if driving range retention becomes less of a concern due to improvements in charging infrastructure.

4.4. Drive Cycle Effects

As mentioned in previous sections, the average speeds and aggressiveness of the drive cycles influenced the energy consumption and calculated range for the test vehicles. The UDDS cycle, for example, being a city-style cycle, includes low speeds and many stops. On the other hand, the HWFET highway cycle has a single stop at the end and relatively high and consistent speeds. Once the cabin temperatures of the vehicles were stabilized, the heating load over both types of test cycles was relatively consistent, as shown in the later cycles in Figure 5. However, the energy consumption associated with the heating system varied significantly due to the drive cycle. This is evident in the later cycles in the test days in Figures 8 and 9, where the heating energy consumption over the UDDS cycles could be over twice that of during the HWFET cycle. This varying energy consumption of each heating system once the cabin had been warmed up is mostly due to the average speed of the cycle and thus the change in the amount of distance covered during the same amount of time. If a longer distance is covered, the denominator in the energy consumption will be larger, and the effect of similar heating loads will be lessened.

4.5. Shield Current Effects

Shield currents were accounted for in this test program using the dual-probe method to eliminate them from the results (see Section 2.6). However, looking back at the raw data, it is possible to determine the magnitude of the shield currents induced in the cables during measurements. This provides a glimpse of the potential magnitude of the errors that would be produced if these shield currents were not accounted for. The maximum shield currents in the rear motor were found to be about 0.4 A. This may not seem like a large amount; however, when multiplied by a battery voltage of around 350 V DC, the cumulative effect of such a current can be significant. In terms of energy over the course of a cycle, the maximum shield-induced error in a single component was about 35 Wh, or about 2.5% of the total cycle energy in a "worst case" scenario. This illustrates the importance of correcting for shield currents when testing electric vehicles with shielded high-voltage cables.

4.6. Certification Results and Discrepancies

For BEV range-labelling purposes, the Canadian and United States regulations require test agencies to combine the UDDS and HWFET ranges (using 55% and 45% weighted average values) and then multiply this computed value by an "adjustment factor" to better estimate real-world performance. Vehicle manufacturers can either use the standard

2-cycle adjustment factor of 0.7 or calculate a 5-cycle adjustment factor (5-cycle factors were used by Tesla for their Model 3 range calculations [39]). In this study, high temperature (35 °C) testing was not performed on either vehicle, so a recalculation of their 5-cycle adjustment factors could not be completed. Therefore, the factors estimated based on certification documents were used instead. Combining the UDDS and HWFET range values at 25 °C with their appropriate weightings and applying the certification adjustment factor for each vehicle (0.70 for Vehicle #1 and 0.73 for Vehicle #2), we obtain range ratings of 441 km and 510 km for Vehicle #1 and Vehicle #2, respectively, based on our chassis dynamometer testing. These values are lower than the vehicles' rated ranges (518 and 576 km, respectively). The lower UBE and different EC_{DC} values measured in this study may account for this discrepancy.

As mentioned in the Section 3.6, the UBEs determined for both vehicles in this study (and used to calculate range) were lower than those published in certification documents, and this may be at least partially attributed to battery degradation over time. When not in use for testing, the BEVs used in this study may not have been charged and used as they would have under typical usage scenarios. This could have led to early battery degradation, since large amounts of time may have been spent at high states of charge (SOCs) while idle. This type of battery degradation could explain the measured UBE being lower than the UBE reported in certification results for both vehicles [40].

In addition, the measured EC_{DC} values used to calculate the vehicles' driving ranges in this study were higher than those published in certification documents, which would reduce the calculated range. This may be the result of differences in laboratory test setups (such as using a chain system versus other dynamometer tie-down methods) and differences in dynamometer loading. Specifically, the set coefficients used for certification and those determined at TEEL show some discrepancy, especially for Vehicle 2. Set coefficients do vary on different chassis dynamometers; however, a wide difference is unusual and could contribute to the higher energy consumption.

Finally, even though the SMCT+ is a newer procedure and aims to obtain similar results to previous methods, the Multi-Cycle Test (MCT) procedure is still the approved method of obtaining city and highway ranges for BEVs [23]. Manufacturers of BEVs use the MCT to determine the vehicles' UBE, range, and energy consumption for certification. Because the SMCT+ procedure was used in this test program, this may have also caused some discrepancy between the driving range figures obtained during certification and those obtained in this test program.

4.7. Policy Implications

The policy implications of this study include the fact that heat pumps can reduce energy consumption of BEVs in cold weather, retaining more driving range and lowering the in-use impact of the vehicle. However, they may not improve performance on cold-start in very cold conditions, and their performance at temperatures colder than those encountered in this study remains to be seen. In addition, different heat pump implementations (using additional backup PTC heaters or different refrigerant types) may have different performance characteristics than those encountered in this study.

4.8. Future Work

The Transportation Emissions and Electrification Laboratory (TEEL) will continue to test electric vehicles at cold temperatures whenever possible to create an internal database of BEV cold weather performance. In addition, novel heating systems (whether they are heat pumps using different refrigerants or completely different technologies) will be sought

out for future testing at the lab. This will inform Canadian regulators about the available technologies for BEV cabin heating and their relative performance in the Canadian climate.

5. Conclusions

Many observations can be drawn from the results of this test program, and the main findings are listed in point form below:

- As expected, heating loads were very high on cold-start at low temperatures, between 4 and 5 kW on average throughout the cold-start UDDS cycles at the lowest temperatures.
- Unexpectedly, the heat pump system used more power than the PTC heater over the first two drive cycles at the coldest test temperature (−10 °C). This may be due to the use of a so-called "lossy" mode of operation that the heat pump can use when high heat is required at low temperatures, which allows the heat pump compressor to produce heat directly from stored electricity but lowers its efficiency significantly. A backup PTC heater may improve this performance at extremely cold temperatures.
- The heating system contribution to energy consumption at cold temperatures was highly dependent on the drive cycle; cycles with higher average speeds (HWFET and US06) led to reduced heating energy consumption, while cycles with lower average speeds (UDDS) led to increased energy consumption for similar levels of average heating power.
- The heat pump reduced the overall energy consumption for all drive cycle types at all cold temperatures when using SAE J1634-type calculations to obtain a single energy consumption result for each drive cycle.
- Calculated range reduction over the UDDS cycle at very cold temperatures for both vehicles was over 50% when compared to the standard temperature (25 °C) UDDS results.
- Neither vehicle achieved its rated driving range at 25 °C (when using their certification adjustment factors and combining UDDS and HWFET results at 55% and 45%, respectively), and this may have been due to differences in test procedures, dynamometer loading, and potential battery degradation in the test vehicles.
- The heat pump-equipped BEV's range retention capability was improved at cold temperatures when compared to the PTC heater-equipped BEV. This improvement varied between 1% and 15%, depending on the cycle and temperature.
- The heat pump-equipped vehicle achieved the most range retention advantage (15% more range retained than the PTC heater-equipped vehicle) at moderate cold temperatures (0 °C) over the UDDS cycle.
- At the coldest condition (−10 °C) over the UDDS cycle, the heat pump-equipped vehicle only achieved a 1% range retention advantage over the PTC heater-equipped vehicle.
- On average, the heat pump-equipped vehicle achieved a 7% range retention advantage on the UDDS cycle, a 7% advantage on the HWFET cycle, and a 4% advantage on the US06 cycle over the PTC-equipped vehicle at all cold temperatures combined. This amount of improvement may be beneficial to users in cold climates, and heat pump systems are already available on many BEVs in Canada.

Author Contributions: Conceptualization, K.H. and A.L.-L.; methodology, K.H. and A.L.-L.; analysis software, K.H.; validation, K.H.; formal analysis, K.H.; writing—original draft preparation, K.H.; writing—review and editing, K.H. and A.L.-L.; visualization, K.H. All authors have read and agreed to the published version of the manuscript.

Funding: This research was jointly funded by two Canadian federal government entities: the Transportation Emissions and Electrification Laboratory (TEEL) at Environment and Climate Change

Canada, and Transport Canada's EcoTechnology for Vehicles (TC-eTV) program. The test vehicles were loaned to TEEL for the duration of testing by the TC-eTV program.

Data Availability Statement: The data used in this paper is not publicly available at this time due to the inclusion of data collected using proprietary databases and the large size of the data files collected.

Acknowledgments: This work is © His Majesty, the King in Right of Canada, as represented by the Minister of the Environment, 11 March 2026. The authors would like to thank the staff of Transport Canada's ecoTechnology for Vehicles program for providing the vehicles used in this test program, as well as the staff of the Transportation Emissions and Electrification Laboratory at Environment and Climate Change Canada for performing the testing described in this report. Special thanks to Maurice Osborne, Lukasz Sikorski, and Hussein Rashid of Environment and Climate Change Canada.

Conflicts of Interest: The authors declare no conflicts of interest. The funders had no role in the design of the study; in the collection, analyses, or interpretation of data; in the writing of the manuscript; or in the decision to publish the results.

Abbreviations

The following abbreviations are used in this manuscript:

A/C	Air Conditioning
AC	Alternating Current
AJE	Average Judicative Element
AWD	All Wheel Drive
BDC	Bidirectional Charger
BEV	Battery Electric Vehicle
BESS	Battery Energy Storage System
CO_2	Carbon Dioxide
COP	Coefficient of Performance
CSC	Constant Speed Cycle
CSC65	Constant Speed Cycle at 65 mph
DC	Direct Current
ECCC	Environment and Climate Change Canada
EPA	United States Environmental Protection Agency
eTV	ecoTechnology for Vehicles
EVSE	Electric Vehicle Supply Equipment
FDP	Full-Depletion Test
FTP	Federal Test Procedure
GHG	Greenhouse Gas
GVWR	Gross Vehicle Weight Rating
HVAC	Heating, Ventilation, and Air Conditioning
HWFET	Highway Fuel Economy Test
ICE	Internal Combustion Engine
ICEV	Internal Combustion Engine Vehicle
KI	Kinetic Intensity
MCT	Multi-Cycle Test
NCA	Nickel Cobalt Aluminum Oxide
OEM	Original Equipment Manufacturer
PDT	Partial-Depletion Test
PKE	Positive Kinetic Energy
PTC	Positive Temperature Coefficient
PWM	Pulse-Width Modulation
SAE	Society of Automotive Engineers
SMCT	Shortened Multi-Cycle Test
SMCT+	Shortened Multi-Cycle Test Plus Steady-State

SOC	State of Charge
TC	Transport Canada
TC-eTV	Transport Canada ecoTechnology for Vehicles
TEEL	Transportation Emissions and Electrification Laboratory
UBE	Usable Battery Energy
UDDS	Urban Dynamometer Driving Schedule

References

1. Humphries, K.; Loiselle-Lapointe, A. A Comparison of Heat Pump and Resistive Heating Impacts on Battery Electric Vehicle Energy Consumption and Range in Cold Temperatures. In Proceedings of the 38th International Electric Vehicle Symposium and Exhibition (EVS38), Gothenburg, Sweden, 15–18 June 2025.
2. Higuchi, Y.; Kobayashi, H.; Shan, Z.; Kuwahara, M.; Endo, Y.; Nakajima, Y. Efficient Heat Pump System for PHEV/BEV. In *SAE Technical Paper*; SAE International: Warrendale, PA, USA, 2017.
3. Tesla Incorporated. Roadster Service Information. 10 February 2017. Available online: https://service.tesla.com/docs/Public/Roadster/ (accessed on 7 March 2026).
4. Umezu, K.; Noyama, H. Air Conditioning System for Electric Vehicles (i-MiEV). In Proceedings of the SAE Automotive Refrigerant & System Efficiency Symposium, Scottsdale, AZ, USA, 27–29 September 2010.
5. Yang, D.; Huo, Y.; Zhang, Q.; Xie, J.; Yang, Z. Recent advances on air heating system of cabin for pure electric vehicles: A review. *Heliyon* **2022**, *8*, e11032. [CrossRef] [PubMed]
6. Leoncini, G.; Mothier, R.; Michel, B.; Clausse, M. A review on challenges concerning thermal management system design for medium duty electric vehicles. *Appl. Therm. Eng.* **2024**, *236*, 121464. [CrossRef]
7. Zhao, C.; Li, Y.; Yang, Y.; Wan, S.; Yu, F.; Yu, C.; Deng, C.; Zhou, A.; Shen, X. Research on electric vehicle range under cold condition. *Adv. Mech. Eng.* **2022**, *14*, 16878132221087083. [CrossRef]
8. Meyer, J.J.; Lustbader, J.; Agathocleous, N.; Vespa, A.; Rugh, J.; Titov, G. Range Extension Opportunities While Heating a Battery Electric Vehicle. In *SAE Technical Paper*; SAE International: Warrendale, PA, USA, 2018.
9. Meyer, N.; Whittal, I.; Christenson, M.; Loiselle-Lapointe, A. The Impact of Driving Cycle and Climate on Electrical Consumption & Range of Fully Electric Passenger Vehicles. In Proceedings of the 26th Electric Vehicle Symposium, Los Angeles, CA, USA, 6–9 May 2012.
10. Christenson, M.; Loiselle-Lapointe, A.; Whittal, I.; Meyer, N. Impact of mileage accumulation, vehicle aging, cold ambient temperature (−7 °C and −18 °C), and driving style on range and energy consumption of two Japanese battery electric passenger vehicles. In Proceedings of the International Electric Vehicle Technology & Automobile Power Electronics Japan Conference, Yokohama, Japan, 22–24 May 2014.
11. My i-MiEV. Mitsubishi i-MiEV Forum. 16 September 2012. Available online: https://myimiev.com/threads/preparation-for-cold-seasons.694/ (accessed on 7 March 2026).
12. My Nissan Leaf. My Nissan Leaf Forum. 25 January 2014. Available online: https://mynissanleaf.com/threads/charging-time-for-s-sv-and-sl-through-110-v-outlet.14068/ (accessed on 7 March 2026).
13. DIYelectriccar. Heating System Design for EV, VerticalScope. 11 October 2013. Available online: https://www.diyelectriccar.com/threads/heating-system-design-for-ev.89907/ (accessed on 7 March 2026).
14. Boeriu, H. BMW Group Innovation Day 2012: Efficient Dynamics, BMWBLOG. 13 September 2012. Available online: https://www.bmwblog.com/2012/09/13/bmw-group-innovation-day-2012-efficient-dynamics/ (accessed on 7 March 2026).
15. Fraser, R. Audi e-Tron—Electro-Mobility, AnyAuto. 1 July 2011. Available online: https://www.anyauto.com.au/audi-e-tron-electro-mobility/ (accessed on 7 March 2026).
16. Kowsky, C.; Wolfe, E.; Leitzel, L.; Oddi, F. Unitary HPAC System. *SAE Int. J. Passener Cars-Mech. Syst.* **2012**, *5*, 1016–1025. [CrossRef]
17. Kondo, T.; Katayama, A.; Suetake, H.; Morishita, M. Development of Automotive Air-Conditioning Systems by Heat Pump Technology. *Mitsubishi Heavy Ind. Tech. Rev.* **2011**, *48*, 27–32.
18. Recurrent. Which Electric Vehicles Have Heat Pumps? Recurrent Motors Incorporated. 2026. Available online: https://www.recurrentauto.com/questions/which-electric-vehicles-have-heat-pumps (accessed on 7 March 2026).
19. CarHub North York Chrysler. What is an Electric Vehicle Heat Pump and How Does it Work? 24 September 2025. Available online: https://www.northyorkchrysler.ca/electric-vehicle-heat-pump-what-how-works/ (accessed on 7 March 2026).
20. Zhang, N.; Lu, Y.; Ouderji, Z.H.; Yu, Z. Review of heat pump integrated energy systems for future zero-emission vehicles. *Energy* **2023**, *273*, 127101. [CrossRef]
21. Mancini, N.; Mardall, J.S.M.; Koplitz, J.; O'Donnell, C.R.; Hanks, D.F.; Li, H. Optimal Source Electric Vehicle Heat Pump with Extreme Temperature Heating Capability and Efficient Thermal Preconditioning. U.S. Patent 10,967,702, 6 April 2021.

22. WeberAuto. Understanding Tesla's Heat Pump System (Youtube). 22 May 2023. Available online: https://www.youtube.com/watch?v=Dujr3DRkpDU (accessed on 15 April 2025).
23. *SAE J1634*; Battery Electric Vehicle Energy Consumption and Range Test Procedure. SAE International: Warrendale, PA, USA, 2021.
24. U.S. Department of Energy. Available online: https://www.fueleconomy.gov (accessed on 17 April 2025).
25. Car and Driver. 2020 Tesla Model 3 Long Range AWD Features and Specs. Available online: https://www.caranddriver.com/tesla/model-3/specs/2020/tesla_model-3_tesla-model-3_2020/412468 (accessed on 24 April 2025).
26. Car and Driver. 2022 Tesla Model 3 Long Range AWD Features and Specs. Available online: https://www.caranddriver.com/tesla/model-3/specs/2022/tesla_model-3_tesla-model-3_2022/426156 (accessed on 24 April 2025).
27. United States Environmental Protection Agency. Application for TESLA, INC. 2020 Model Year Test Group LTSLV00.0L23 (Update). 27 October 2019. Available online: https://dis.epa.gov/otaqpub/display_file.jsp?docid=48711&flag=1 (accessed on 24 April 2025).
28. United States Environmental Protection Agency. Application for TESLA, INC. 2022 Model Year Test Group NTSLV00.0L23. 23 September 2021. Available online: https://dis.epa.gov/otaqpub/display_file.jsp?docid=54290&flag=1 (accessed on 24 April 2025).
29. Natural Resources Canada. Fuel Consumption Ratings Search Tool, Natural Resources Canada. Available online: https://fcr-ccc.nrcan-rncan.gc.ca/en/ (accessed on 2 February 2020).
30. United States Environmental Protection Agency. Annual Certification Data for Vehicles, Engines, and Equipment—Light-Duty Vehicles and Trucks Certification Data Spreadsheets. 15 December 2025. Available online: https://www.epa.gov/compliance-and-fuel-economy-data/annual-certification-data-vehicles-engines-and-equipment (accessed on 22 January 2026).
31. *SAE J2264*; Chassis Dynamometer Simulation of Road Load Using Coastdown Techniques. SAE International: Warrendale, PA, USA, 2023.
32. O'Keefe, M.P.; Simpson, A.; Kelly, K.J. Duty Cycle Characterization and Evaluation Towards Heavy Hybrid Vehicle Applications. In Proceedings of the SAE World Congress and Exhibition, Detroit, MI, USA, 16–19 April 2007.
33. Jaguemont, J.; Boulon, L.; Dubé, Y. A comprehensive review of lithium-ion batteries used in hybrid and electric vehicles at cold temperatures. *Appl. Energy* **2016**, *164*, 99–114. [CrossRef]
34. Zou, H.; Huang, G.; Shao, S.; Zhang, X.; Tian, C.; Zhang, X. Experimental Study on Heating Performance of an R1234yf Heat Pump System for Electric Cars. In Proceedings of the 9th International Conference on Applied Energy, Cardiff, UK, 21–24 August 2017.
35. Weissler, P. Electric Radiant Heat for EV Cabin Comfort. 19 May 2022. Available online: https://www.sae.org/news/2022/05/electric-radiant-heat-for-ev-cabin-comfort (accessed on 9 April 2025).
36. Mandev, E.; Ceviz, M.A.; Afshari, F.; Muratçobanoğlu, B. Evaluating PCM heat battery as a range-saving solution for electric vehicle cabin heating. *Sustain. Energy Technol. Assess.* **2025**, *76*, 104270. [CrossRef]
37. Liu, C.; Zhang, Y.; Gao, T.; Shi, J.; Chen, J.; Wang, T.; Pan, L. Performance evaluation of propane heat pump system for electric vehicle in cold climate. *Int. J. Refrig.* **2018**, *95*, 51–60. [CrossRef]
38. Motavalli, J. Inside the Quiet, Never-Ending Battle over Automotive Refrigerants. 1 November 2024. Available online: https://www.sae.org/news/2024/11/refrigerant-fight (accessed on 9 April 2025).
39. United States Environmental Protection Agency; United States Department of Energy. Download Fuel Economy Data—Datasets and Guides for Individual Model Years, 2020 and 2022. Available online: https://www.fueleconomy.gov/feg/download.shtml (accessed on 4 February 2026).
40. Loiselle-Lapointe, A.; Guay, L.; Meloche, E. Separating the Effects of Calendar Ageing and Mileage Accumulation on Battery Degradation from a Pair of Light-Duty BEVs. In Proceedings of the 38th International Electric Vehicle Symposium and Exhibition (EVS38), Gothenburg, Sweden, 15–18 June 2025.

Disclaimer/Publisher's Note: The statements, opinions and data contained in all publications are solely those of the individual author(s) and contributor(s) and not of MDPI and/or the editor(s). MDPI and/or the editor(s) disclaim responsibility for any injury to people or property resulting from any ideas, methods, instructions or products referred to in the content.